$A_{15}Tl_{27}$ (A = Rb, Cs): A Structural Type Containing Both Isolated Clusters and Condensed Layers Based on the Tl_{11} Fragment. Syntheses, Structure, Properties, and Band Structure

Zhen-Chao Dong and John D. Corbett*

Ames Laboratory−DOE[1] and Department of Chemistry, Iowa State University, Ames, Iowa 50011

Received August 18, 1995[⊗]

The isomorphous title compounds (and the ordered substitutional $Rb_{14}CsTl_{27}$) are obtained directly from reactions of the elements in sealed Ta below ~330 °C. Refinements of single-crystal data for the three established a structure with alternate layers of isolated pentacapped trigonal prismatic Tl_{11}^{7-} (D_{3h}) ions and condensed $^{2}_{\infty}[Tl_{16}^{8-}]$ networks that are separated by cations. The condensed layer consists of Tl_{11} units that share prismatic edges and are interbridged through waist-capping atoms ($Tl_{6/2}Tl_3Tl_2$). ($Rb_{15}Tl_{27}$: $P\bar{6}2m$, $Z = 1$, $a = 10.3248(6)$ Å, $c = 17.558(2)$ Å.) The rubidium phase is a poor metal ($\rho_{293} \sim 34$ $\mu\Omega$·cm) and is Pauli-paramagnetic. Extended Hückel band calculations indicate partially filled bands and a non-zero DOS at E_F, consistent with the observed metallic behavior, although appropriate cation tuning or modest anion doping should provide a Zintl phase. The band structure and COOP curves are also used to rationalize the distortion of the Tl_{11} unit on condensation and the critical role of the interfragment bonds between waist-capping atoms in stabilizing the layer.

Introduction

Extended structures are very common in the elemental boron, metallic borides,[2] gallides,[3] aluminides,[4,5] and indides.[6−8] Similar reports in alkali metal−thallium systems are relatively rare, amounting to mainly CsCl-type LiTl (Tl−Tl = 3.43 Å),[9] $ZrSi_2$-type Li_2Tl with infinite chains,[10] stuffed diamond-like NaTl (Tl−Tl = 3.24 Å),[11] and the $K_3Na_{26}In_{48}$[6]-related $K_{49}Tl_{108}$ with linked icosahedra and chains of approximate hexagonal antiprisms.[12] While recent investigations have greatly expanded the family of discrete thallium clusters over a nuclearity range of 4−13,[13−18] a few condensed phases have also been identified, e.g., the thallium-richest K_6Tl_{17} with an unusual layered structure and A_4Tl_{13} (A = Rb, Cs) with pentagonal antiprismatic chains.[19] Isolated Tl_{11}^{7-} clusters are the sole units in A_8Tl_{11} (A = K, Rb, Cs),[16,17] and are observed in conjunction with both isolated Au-substituted $Tl_9Au_2^{9-}$ polyanions in $K_{18}Tl_{20}Au_3$[20] and a layered network containing pentagonal bipyramids Cd_5Tl_2 in $K_{14}Cd_9Tl_{21}$.[21] We report here a novel structure shared by $A_{15}Tl_{27}$ (A = Rb, Cs) and $Rb_{14}CsTl_{27}$ in which the same isolated clusters coexist with the condensed layers built from similar Tl_{11} fragments. Semiempirical tight-binding band calculations were performed for $Rb_{15}Tl_{27}$ to rationalize the bonding and to correlate the structure with the observed electrical and magnetic properties.

Experimental Section

Syntheses. All the syntheses were performed by reaction of the constituent elements in welded Ta tubing as described elsewhere.[14] The surfaces of a Tl metal bar (99.998%, Johnson-Matthey) were cleaned with a scalpel before use, while the Rb (99.9%, Alfa) and Cs (99.98%, Johnson-Matthey) received sealed under Ar were used as is. Because both the reagents and products are very sensitive to air and moisture, all operations were carried out in a N_2- or He-filled glovebox with typical humidity levels less than 0.1 ppm (vol).

The title compounds $A_{15}Tl_{27}$ (hereafter denoted 15−27) were presumably those reported as "ATl_2" for both Rb and Cs according to the 1970 phase diagrams obtained from thermal analyses by Thümmel and Klemm.[22] Both are incongruently melting according to these, with peritectic temperatures of ~335 and 350 °C respectively. Syntheses from stoichiometric proportions in Ta containers at 500 °C followed by slow cooling yield the 15−27 compounds as a major phase with A_4Tl_{13} as a byproduct. Numerous platelike crystals were formed with a shiny metallic luster. A reaction was also carried out for $Rb_{14}CsTl_{27}$, a unique composition deduced from the established 15−27 structure. Pure phases for all three were later obtained by annealing the stoichiometric mixtures at 250 °C for 30 days.

X-ray powder patterns for samples mounted between pieces of cellophane were collected with the aid of an Enraf-Nonius Guinier camera, Cu Kα radiation ($\lambda = 1.540\,562$ Å), and NBS (NIST) silicon as an internal standard. Least-square refinements of 64−77 lines indexed on the basis of the refined structural model resulted in the lattice constants given in Table 1. The $A_{15}Tl_{27}$ compounds appear to be line phases, as mixtures with different overall compositions gave the same cell parameters with deviations less than 0.005 Å (6σ) for Rb and Cs.

Property Measurements. The resistivity of pure $Rb_{15}Tl_{27}$ was examined by the electrodeless "Q" method[23] for a 98-mg sample that

⊗ Abstract published in *Advance ACS Abstracts,* February 15, 1996.
(1) This research was supported by the Office of the Basic Energy Sciences, Materials Sciences Division, U.S. Department of Energy. The Ames Laboratory is operated for DOE by Iowa State University under Contract No. W-7405-Eng-82.
(2) Matkovich, V. I. Ed. *Boron and Refractory Borides*; Springer-Verlag: Berlin, 1977.
(3) Belin, C.; Tillard-Charbonnel, M. *Prog. Solid State Chem.* **1993**, *22*, 59.
(4) Kreiner, G.; Franzen, H. F. *J. Alloys Compd.* **1995**, *221*, 15.
(5) Häussermann, U.; Wengert, S.; Nesper, R. *Angew. Chem., Int. Ed. Engl.* **1994**, *33*, 2069.
(6) Sevov, S. C.; Corbett, J. D. *Inorg. Chem.* **1993**, *32*, 1612.
(7) Sevov, S. C.; Corbett, J. D. *Inorg. Chem.* **1992**, *31*, 1895.
(8) Sevov, S. C.; Corbett, J. D. *Science*, **1993**, *262*, 880.
(9) Zintl, E.; Brauer, G. *Z. Phys. Chem.* **1933**, *20B*, 245.
(10) Stöhr, J.; Müller, W.; Shäfer, H. *Acta Crystallogr.* **1981**, *37A*, C-185.
(11) Zintl, E.; Dullenkopf, W. *Z. Phys. Chem.* **1932**, *B16*, 195.
(12) Cordier, G.; V. Müller, V.; Fröhlich, R. *Z. Kristallogr.* **1993,** *203*, 148.
(13) Hansen, D. A.; Smith, J. F. *Acta Crystallogr.* **1967,** *22*, 836.
(14) Dong, Z.-C.; Corbett, J. D. *J. Am. Chem. Soc.* **1994**, *116*, 3429.
(15) Dong, Z.-C.; Corbett, J. D. *J. Am. Chem. Soc.* **1993**, *115*, 11299.
(16) Dong, Z.-C.; Corbett, J. D. *J. Cluster Sci.* **1995**, *6*, 187.
(17) Cordier, G.; V. Müller, V. *Z. Kristallogr.* **1992**, *198*, 281.
(18) Dong, Z.-C.; Corbett, J. D. *J. Am. Chem. Soc.* **1995**, *117*, 6447.
(19) Dong, Z.-C.; Corbett, J. D. Unpublished research.
(20) Dong, Z.-C.; Corbett, J. D. *Inorg. Chem.* **1995**, *34*, 5042.
(21) Tillard-Charbonnel, M.; Chahine, A.; Belin, C. *Z. Kristallogr.* **1995**, *210*, 162.
(22) Thümmel, R.; Klemm, W. *Z. Anorg. Allg. Chem.* **1970**, *376*, 44.

0020-1669/96/1335-1444$12.00/0

Table 1. Selected Data Collection and Refinement Parameters for $Rb_{15}Tl_{27}$, $Rb_{14}CsTl_{27}$, and $Cs_{15}Tl_{27}$

formula	$Rb_{15}Tl_{27}$	$Rb_{14}CsTl_{27}$	$Cs_{15}Tl_{27}$
fw	6800.01	6847.44	7511.57
space group, Z	$P\bar{6}m$ (No. 189), 1	$P\bar{6}2m$ (No. 189), 1	$P\bar{6}2m$ (No. 189), 1
lattice params,[a] Å			
a	10.3248(6)	10.3519(6)	10.503(1)
c	17.558(2)	17.545(2)	18.142(2)
V, Å^3	1621.0(3)	1628.3(3)	1733.2(4)
ρ_{calcd}, g/cm^3	6.965	6.983	7.196
no. of indep obsd reflns	495 ($I \geq 3\sigma(I)$)	318 ($I \geq 2\sigma(I)$)	306 ($I \geq 3\sigma(I)$)
μ, cm^{-1} (Mo Kα)	783.33	778.61	708.42
transm range	0.37−1.25	0.76−1.20	0.37−1.19
residuals: R; R_w[b]	0.049; 0.048	0.063; 0.045	0.062; 0.064

[a] Guinier data, λ = 1.540 562 Å, 23 °C. [b] $R = \sum||F_o| - |F_c||/\sum|F_o|$; $R_w = [\sum_w(|F_o| - |F_c|)^2/\sum w(F_o)^2]^{1/2}$; $w = 1/\sigma^2$.

had been sieved to 250−400 μm and diluted with chromatographic Al_2O_3. Measurements were made at 34 MHz over the range of 100−293 K. Magnetic susceptibilities were also measured for $Rb_{15}Tl_{27}$ (25 mg) at 0.01 and 3 T over 6−300 K on a Quantum Design MPMS SQUID magnetometer. The raw data were corrected for the susceptibility of the container and for the diamagnetism of the cores[24] as well as for the Larmor precession contribution of the delocalized valence electrons in the skeletal orbitals in the isolated cluster.[14,25]

Structure Determination. Platelike crystals of $Rb_{15}Tl_{27}$, $Cs_{15}Tl_{27}$, and $Rb_{14}CsTl_{27}$ were picked up and sealed in thin-walled capillaries and then checked by Laue or oscillation photography for their singularity. Intensity data were collected on an Enraf-Nonius CAD-4 diffractometer with graphite-monochromated Mo Kα radiation at 23 °C. Programmed indexing of 25 reflections from a random search over $14 \leq 2\theta \leq 30°$ yielded the same primitive hexagonal cells for all three. Two octants of data were measured in each case in an $\omega-2\theta$ scan mode for 2θ up to 60° for $Cs_{15}Tl_{27}$, 55° for $Rb_{15}Tl_{27}$, and 50° (default value) for $Rb_{14}CsTl_{27}$. Assignment of the space group $P\bar{6}2m$ was made on the basis of the systematic absences and statistical analyses of intensity distribution, and was supported by the subsequent successful refinements. The structure was solved by the direct methods via SHELXS-86.[26] Peak assignments were easily made in terms of both bond distances and peak heights. The serious absorption effects, with linear absorption coefficients around 780 cm^{-1}, were in each case corrected empirically according to, first, the average of the ψ-scan curves for five to eight strong reflections at different θ values and, subsequently, by DIFABS after the isotropic refinements converged (as recommended).[27] Multiplicity refinements of Tl atoms (B's varying) with the alkali-metal atoms fixed indicated that these sites are fully occupied with deviations from unity of less than 3σ. The inverse procedure gave the same answer for alkali-metal atoms, including the unique Cs in $Rb_{14}CsTl_{27}$. All data reduction and structure refinements were performed using the TEXSAN package[28] on a VAX station. The data collection and refinement parameters are listed in Table 1. Because of the isostructural character of the three 15−27 compounds and the somewhat poorer refinements obtained for $Cs_{15}Tl_{27}$ and $Rb_{14}CsTl_{27}$ (insufficient observed reflections owing to weaker X-ray diffraction by the crystal of the former and the lower 2θ limit for the latter), the atomic positional and isotropic thermal parameters as well as the important interatomic distances for only $Rb_{15}Tl_{27}$ are listed in Tables 2 and 3, respectively. The environments about the A4 cations need special attention and are listed for all three phases in Table 4. The rest of crystallographic details, positional and distance data for the other two compounds, and anisotropic displacement parameters for all three are contained in the supporting information; these as well as the structure factor data are also available from J.D.C.

Table 2. Positional Coordinates and Isotropic Thermal Parameters for $Rb_{15}Tl_{27}$

atom	x	y	z	B_{eq},[a] Å^2
Tl1	0	0	0.1510(5)	2.1(2)
Tl2	0.7877(5)	0	0	2.0(3)
Tl3	0.2855(3)	0	0.0911(2)	2.1(2)
Tl4	0.1719(4)	0.4639(4)	$^1/_2$	2.1(1)
Tl5	0.6199(4)	0	0.3995(2)	2.7(2)
Tl6	$^1/_3$	$^2/_3$	0.3434(3)	2.2(1)
Rb1	0.612(1)	0	0.1844(6)	3.2(5)
Rb2	$^2/_3$	$^1/_3$	0	3.2(6)
Rb3	0.270(1)	0	0.3108(6)	2.8(5)
Rb4	0	0	$^1/_2$	4(1)

[a] $B_{eq} = (8\pi^2/3)\sum_i\sum_j \mathbf{U}_{ij}a_i^*a_j^*\vec{a}_i\vec{a}_j$.

Table 3. Bond Distances in $Rb_{15}Tl_{27}$ (<5 Å)

Tl1−Tl2 3×	3.440(7)	**Tl6**−Tl4 3×	3.351(5)
Tl1−Tl3 3×	3.130(5)	Tl6−Tl5 3×	3.374(3)
Tl1−Rb1 3×	4.05(1)	Tl6−Rb1 3×	4.246(8)
Tl1−Rb3 3×	3.96(1)	Tl6−Rb3 3×	3.852(6)
Tl2−Tl1 2×	3.440(7)	**Rb1**−Tl1	4.05(1)
Tl2−Tl2 2×	3.796(9)	Rb1−Tl2	3.71(1)
Tl2−Tl3 4×	3.097(3)	Rb1−T13	3.75(1)
Tl2−Rb1 2×	3.71(1)	Rb1−T13 2×	3.949(8)
T12−Rb2 2×	4.208(4)	Rb1−T15	3.78(1)
		Rb1−Tl6 2×	4.246(8)
Tl3−Tl1	3.130(5)	Rb1−Rb2 2×	4.551(8)
Tl3−Tl2 2×	3.097(3)	Rb1−Rb3	4.17(1)
Tl3−Tl3	3.199(8)	Rb1−Rb3 2×	4.192(9)
Tl3−Rb1	3.75(1)		
Tl3−Rb1 2×	3.949(8)	**Rb2**−T12 3×	4.208(4)
Tl3−Rb2 2×	4.043(3)	Rb2−T13 6×	4.043(3)
Tl3−Rb3	3.86(1)	Rb2−Rb1 6×	4.551(8)
T14−T14	3.073(7)[a]	**Rb3**−T11	3.96(1)
T14−T14 2×	3.319(6)	Rb3−T13	3.86(1)
T14−T15 2×	3.442(5)	Rb3−T14 2×	3.825(9)
T14−T15 2×	3.216(4)	Rb3−T15	3.93(1)
T14−T16 2×	3.351(5)	Rb3−T15 2×	3.830(6)
T14−Rb3 2×	3.825(9)	Rb3−T16 2×	3.852(6)
T14−Rb4	4.194(4)	Rb3−Rb1	4.17(1)
		Rb3−Rb1 2×	4.192(9)
T15−T14 2×	3.422(5)	Rb3−Rb3 2×	4.83(2)
T15−T14 2×	3.216(4)	Rb2−Rb4	4.34(1)
T15−T15	3.528(9)		
T15−T16 2×	3.374(3)	**Rb4**−T14 6×	4.194(4)
T15−Rb1	3.78(1)	Rb4−T15 6×	4.303(4)
T15−Rb3	3.93(1)	Rb4−Rb3 6×	4.34(1)
T15−Rb3 2×	3.830(6)		
T15−Rb4	4.303(4)		

[a] Interfragment Tl4−Tl4 distance.

Results and Discussion

Cluster Skeletons. The most unusual features of this structure are, first, the coexistence of isolated clusters with two-dimensional condensed layers, and second, the evident use of the *same* Tl_{11} skeleton in both parts (Figure 1). The latter appears to make it unique not only among the A−Tr phases (A = alkali metal; Tr = B, Al, Ga, In, Tl), but also in other

(23) Shinar, J.; Dehner, B.; Beaudry, B. J.; Peterson, D. T. *Phys. Rev.* **1988**, *37B*, 2066.
(24) Selwood, P. W. *Magnetochemistry*, 2nd ed.; Interscience Publishers: New York, 1956; p 70.
(25) Ashcroft, N. W.; Mermin, D. N. *Solid State Physics*; Holt, Rinehart and Winston: Philadelphia, PA, 1976; p 649.
(26) Sheldrick, G. M. SHELXS-86. Universität Göttingen, Germany, 1986.
(27) Walker, N.; Stuart, D. *Acta Crystallogr.* **1986,** A39, 158.
(28) TEXSAN, version 6.0 package. Molecular Structure Corp., The Woodlands, TX, 1990).

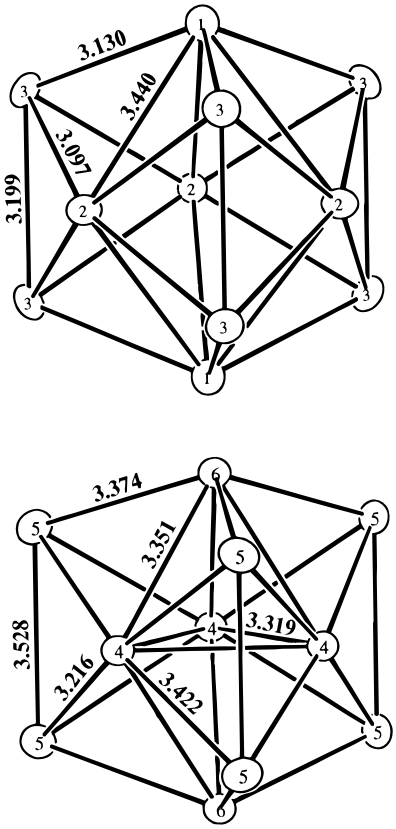

Figure 1. Cluster units in $Rb_{15}Tl_{27}$. Top: the isolated Tl_{11}^{7-} polyanion (D_{3h}); Bottom: the Tl_{11} cluster fragment (C_{3h}) in the two-dimensional condensed layer (50% probability thermal ellipsoids).

Table 4. Environment of the A4 Atom (Distances in Å) in $Rb_{15}Tl_{27}$, $Rb_{14}CsTl_{27}$ (A4 = Cs), and $Cs_{15}Tl_{27}$

	$Rb_{15}Tl_{27}$	$Rb_{14}CsTl_{27}$	$Cs_{15}Tl_{27}$
A4−Tl4 6×	4.194(4)	4.211(7)	4.31(1)
A4−Tl5 6×	4.302(4)	4.332(7)	4.42(1)
A4−A3 6×	4.34(1)	4.35(1)	4.42(2)

intermetallic systems. Otherwise, size and electronic tuning of the other cluster anions has produced the same isolated Tl_{11}^{7-} cluster units in $K_{18}Tl_{20}Au_3$[20] and $K_{14}Cd_9Tl_{21}$[21] plus isolated $Tl_9Au_2^{9-}$ clusters in the former and condensed Cd_5Tl_2 layers in the latter. The principal geometric characteristics of Tl_{11}^{7-}, as described before,[16,29] is a pronounced compression of the "ideal" 11-atom model along the 3-fold axis accompanied by a significant basal expansion. The overall differences between the Tl_{11}^{7-} units in A_8Tl_{11} (A = K, Rb, Cs) and the present examples are extremely small except the point group symmetry increases from D_3 to D_{3h}, which makes all waist to prism (Tl2-Tl3) distances equivalent (3.097 Å vs an average of 3.058 and 3.150 Å in A_8Tl_{11}). The different Tl−Tl separations range from 3.097(3) to 3.440(7) Å with an average 3.253(5) Å over the polyhedron, the same as the 3.26 Å average over A_8Tl_{11}. These small changes are presumably all related to packing effects.

What strikes one most is that similar Tl_{11} fragments can be viewed as building blocks in the condensed layers through (a) sharing the three parallel edges of the trigonal prism, and (b) formation of exo intercluster bonds between waist atoms (Tl4−Tl4, Figures 1 and 2). Referred to the isolated Tl_{11}^{7-} (D_{3h}) cluster, the dimensions of the Tl_{11} (C_{3h}) unit in the layer have been altered during the condensation, with the waist-capping atoms moving significantly inward to each other, from 3.796(9) to 3.319(6) Å. Correspondingly, the prism height (Tl5−Tl5) is stretched from 3.199(8) to 3.528(9) Å, the axial separation (Tl6−Tl6) increased in parallel from 5.30(1) to 5.60(1) Å, and the basal plane edges of the prism expanded from 5.106(6) to 5.590(3) Å. In this sense, an alternate description of the fragment condensed is a hexacapped trigonal bypyramid (In4, In6) which generates the network through waist exo bonding and sharing of all capping atoms. The distances around the shared Tl5 atom increase, as expected, because of the larger number of Tl neighbors (7 vs 4). Since each Tl_{11} unit is connected to three neighboring fragments related by a 3-fold axis, condensation naturally results in a geometry with six-member rings and close to graphite-like layers. Also noteworthy are the exo Tl4−Tl4 intercluster connections (the thicker bonds in Figure 2), the shortest Tl−Tl distance (3.073(7) Å) in the structure. The Tl4 atoms are also not centered on each Tl5 rectangular face, but shifted so as to lengthen this short intercluster Tl4−Tl4 bond. This distortion lowers the point group symmetry of the Tl_{11} unit from D_{3h} to C_{3h} and results in two types of Tl4−Tl5 distances with the shorter 3.216 Å distance on the face of the cavity and the longer 3.422 Å distance buried inside the framework. A distantly related example of the metal framework can be found in $M_2Ta_9S_6$ (M = Fe, Co, Ni) when the structures are viewed along the *c* direction, in which the condensed metal clusters can be derived from M-centered tricapped trigonal prisms of Ta by sharing faces along the *c* axis and waist-capping Ta atoms normal to that.[30] But these are three-dimensional condensed structures and even the building blocks and sharing features are different. The present layered structure appears to be the first example in terms of either the building blocks or the way they are connected. The structural formula for the Tl sublattice may be written as $[Tl_{11}]$ plus $^{2}_{\infty}[Tl_{6/2}Tl_{3/1}Tl_{2/1}]_2$ ($\equiv Tl_{27}$).

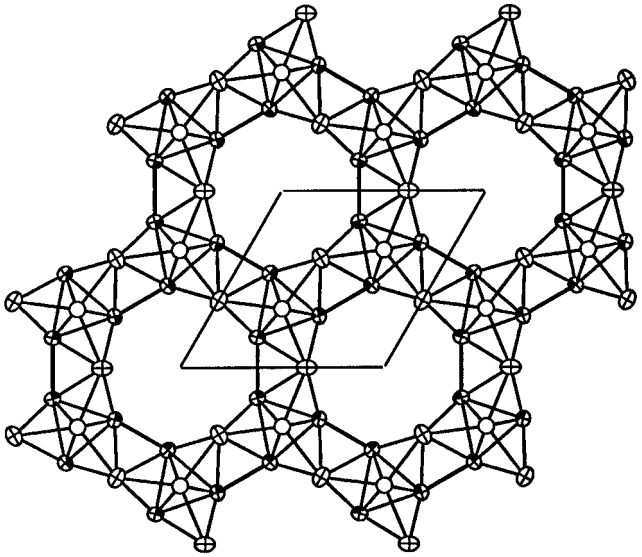

Figure 2. [001] projection of the condensed thallium layer in $Rb_{15}Tl_{27}$ showing the prism edge-sharing (Tl5−Tl5) and the intercluster waist Tl4−Tl4 connections (thick bonds, 3.073(7) Å). Shaded ellipsoids stand for waist Tl4, crossed circles for prismatic Tl5, and open circles for axial Tl6. (90%)

Cation Distributions and Cluster Packing. Figure 3 shows the space partitioning among isolated clusters, condensed cluster layers, and the "solvating" cations in a unit cell. The top view illustrates how the isolated clusters are located directly above and below the cavities within the condensed layer (the intercluster Tl4−Tl4 bonds are not drawn in this figure), while the bottom view indicates the alternate hexagonal stacking of the isolated cluster "layer" and the condensed cluster layer along the *c* axis. The effort to follow closed packing principles and

(29) Sevov, S. C.; Corbett, J. D. *Inorg. Chem.* **1991**, *30*, 4875.

(30) Harbrecht, B.; Franzen, H. F. *J. Less-Common Met.* **1986**, *115*, 177.

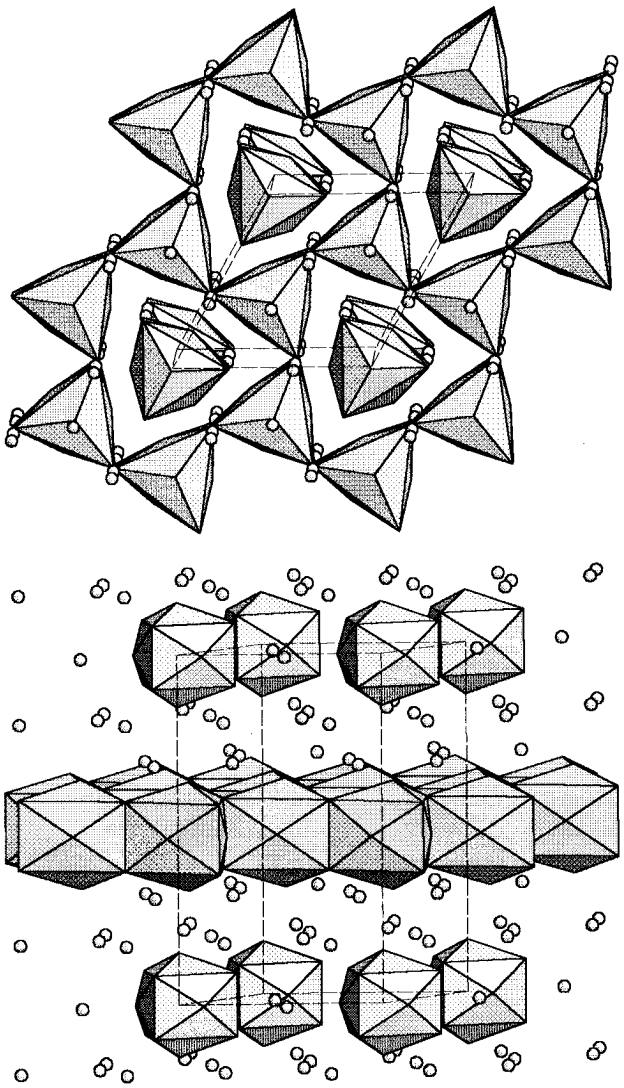

Figure 3. Distribution of isolated Tl_{11}^{7-} polyanions, condensed thallium layers, and solvating cations in $Rb_{15}Tl_{27}$ with the unit cell marked. Top: approximate [001] projection. Bottom: approximate [100] view with cations as small circles. The alternating hexagonal stacking of the isolated "layer" with the condensed layer along the *c* direction as well as the double Rb layers between the neighboring thallium layers are evident.

the substantial "solvation" of anion networks by alkali-metal cations are evident. The double alkali-metal layers (Rb1 and Rb3) nicely separate the isolated clusters from the condensed cluster layer. The shortest intercluster distance between these two is 5.781(5) Å between Tl3 and Tl6, which is far enough to exclude any substantial interaction.

Another aspect of the structure worth mentioning is the cavity defined by the six-member ring of Tl_{11} fragments. The Rb4 atom at the center (D_{3h}) has two types of Tl coordinations, six of each at 4.19 and 4.30 Å, together with six distant Rb3 neighbors (Figure 4). However, judging from the average A−Tl distances of 3.94 and 4.08 Å for Rb and Cs in A_8Tl_{11} respectively,[16] the cavity is too large for Rb, which accounts for its larger thermal parameter (4 $Å^2$) with respect to other Rb atoms. A straightforward prediction of Cs atom substitution for Rb4 was confirmed by the subsequent stoichiometric synthesis of $Rb_{14}CsTl_{27}$ and a single crystal study. Table 4 lists the A4 neighbor distances for all three compounds, which indicate that while the Cs atom inside the cavity has little effect on the overall structure, the Cs atoms lying between cluster layers increase the A4 cavity slightly because of their larger cation size and resultant packing requirements. This in turn

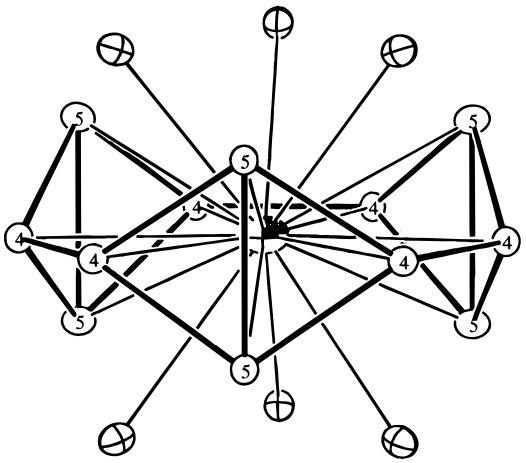

Figure 4. Environment around the Rb4 cation in $Rb_{15}Tl_{27}$. Labeled open circles stand for Tl, and crossed circles, for Rb3. (50%).

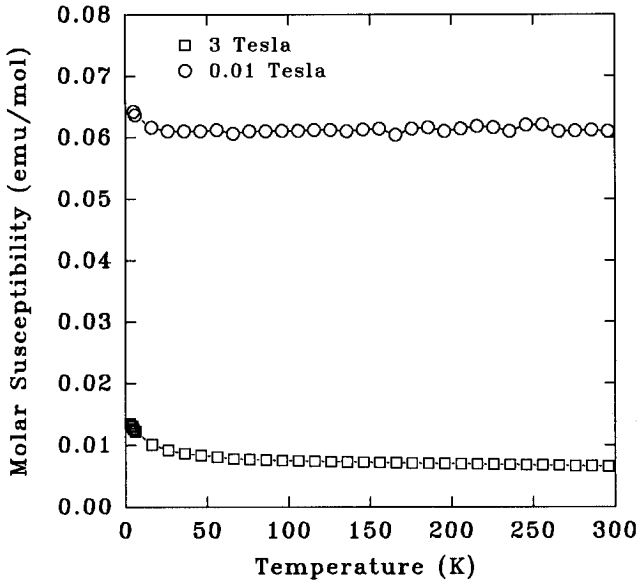

Figure 5. Temperature dependence of the molar susceptibility of $Rb_{15}Tl_{27}$ over 6−300 K at 0.01 and 3 T.

makes the hole even too large for Cs (also revealed by its large B_{eq} value).

The specific roles of the cations about the cluster faces, edges, and vertices are to compensate anionic charge and to bridge between clusters. As in A_8Tl_{11} (A = K, Rb, Cs),[16] the isolated Tl_{11}^{7-} cluster is surrounded by 24 alkali-metal atoms with very similar functions. Six waist Tl2−Tl3−Tl3 triangles are each capped by a Rb2 atom that is in turn shared by two other waist triangles of the neighboring clusters, while each end of Tl_{11}^{7-} is capped, bridged, and exo-bonded by Rb1 (μ_4 to Tl1−Tl3−Tl2−Tl3), Rb3 (μ_2 to Tl1−Tl3), and Rb1 (to Tl3), respectively, three of each type. The cation environment around the condensed Tl_{11} unit does not differ too much from the isolated unit, except six waist-capping positions are alternatively occupied by the Rb4 and waist capping Tl4 atoms in the neighboring cluster units, and the Rb1 and Rb3 atoms have alternate solvation functions in the cluster and the layer.

Properties and Bonding. Magnetic susceptibility data for $Rb_{15}Tl_{27}$ at 0.01 and 3 T are shown in Figure 5. Diamagnetic corrections have been applied to exclude the contributions from the cores[24] (-12.18×10^{-4} emu/mol) and the Larmor precession[25] (-2.78×10^{-4} emu/mol) of the skeletal electrons in the isolated Tl_{11}^{7-} clusters. The compound shows a substantially temperature-independent susceptibility above ~ 50 K, a Pauli-paramagnetic property of $\sim 7 \times 10^{-3}$ emu/mol (or 7×10^{-6}

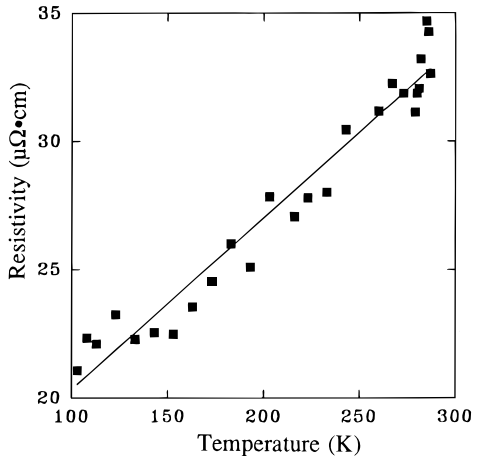

Figure 6. Resistivity of $Rb_{15}Tl_{27}$ vs temperature over 100−293 K by the "Q"-method.

emu/cm^3) at 3 T. A picture with conduction electrons but no localized unpaired spins in the structure is thus implied. As usual, the susceptibilities decrease with increase of the field, as has been explained elsewhere.[20] Consistent with the magnetic properties, the temperature-dependence resistivity data in Figure 6 indicate a metallic behavior with $\partial\rho/\rho\partial T = +0.20(1)\%\ K^{-1}$ and $\rho_{293} \sim 34\ \mu\Omega$·cm.

In order to better understand the structure and properties as well as their interrelations, electronic structure calculations were performed on both the observed Tl_{11}^{7-} cluster and two-dimensional Tl_{11}-based layer with extended Hückel tight-binding methods.[31,32] The validity of the extended Hückel calculations in such a system and the justification of the atomic parameters used for Tl (6s, $\zeta = 2.14$, $H_{ii} = -11.60$ eV; 6p, $\zeta = 2.04$, $H_{ii} = -5.80$ eV) were described in previous papers.[15,18] Relativistic effects[33] will definitely modify the individual energy levels of Tl because of the spin−orbit splitting of $6p_{1/2}$ and $6p_{3/2}$ (∼0.95 eV in Tl(g)). But, as concluded before,[18] the general bonding picture will still remain basically the same as found from a routine extended Hückel calculation because of mixing of the p levels, and thus relativistic effects are not our concern for the present. The effects of alkali-metal cations and isolated Tl_{11}^{7-} clusters on the electronic structure of the condensed layer were not taken into account either, because the cation states are generally considered to be high-lying, and the Tl−Tl interactions among isolated clusters or with the layer should be much weaker in comparison with the interactions within the condensed layer.[34,35] Thus, band calculations were performed only on the condensed thallium layer with $[Tl_{6/2}Tl_{3/1}Tl_{2/1}]_2$ ($\equiv Tl_{16}$) as the independent unit (the unit cell projection in Figure 2). DOS and COOP curves[36] were evaluated from 300 k points in the two-dimensional Brillouin zone with the special k points Γ (0, 0), M ($a^*/2$, 0), and K ($a^*/3$, $b^*/3$). Tight-binding overlaps were included within two neighboring cells along a and b directions.

The bonding picture within the hypoelectronic Tl_{11}^{7-} has been well established for A_8Tl_{11} (A = K, Rb, Cs)[16] and A_8In_{11};[29,35] that is, an isolated Tl_{11}^{7-} polyanion has the optimum electronic configuration with the first 20 valence MOs filled and a HOMO−LUMO gap of ∼0.70 eV. On the other hand, the bonding and electron count are not so straightforward for the condensed thallium layer. Figures 7−9 show the band structure along the symmetry lines (the predominantly 6s-based bands below −8 eV are omitted), projections of various Tl contributions on the total DOS, and the overlap-weighted population, i.e., COOP, curves for various components, respectively. Since the mirror symmetry is always present over the Brillouin zone, it is used to determine whether a band is *symmetric (S)* or *antisymmetric (A)*. The dependencies of the Fermi energy and overlap populations on valence electron counts (VEC) are given in Table 5.

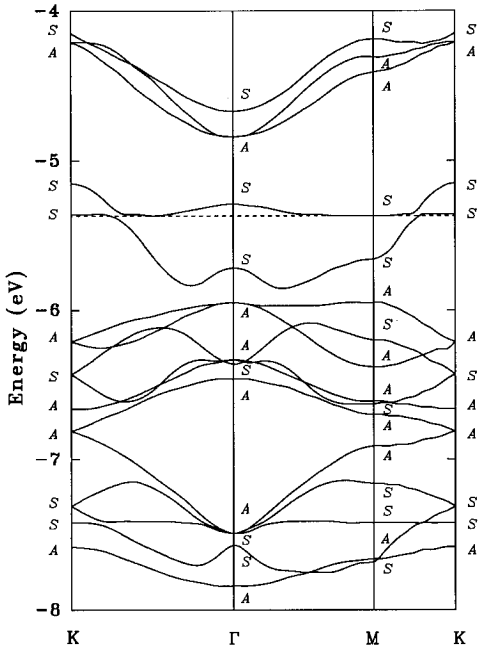

Figure 7. Predominantly p-based band structure for the condensed thallium layer in $Rb_{15}Tl_{27}$. The dashed line marks the Fermi energy ($E_F = -5.37$ eV).

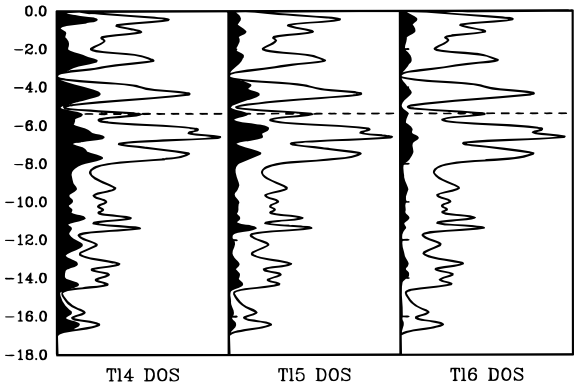

Figure 8. Projections of the constituent thallium atom contributions to the total DOS within the condensed layer in $Rb_{15}Tl_{27}$.

The band structure together with the overlap-weighted populations indicate a closed shell $^2_\infty[Tl_{16}^{6-}]$ anion configuration, with the first 27 bands filled (VEC = 54, $E_F = -5.95$ eV), although the band structure alone suggests an alternate $^2_\infty[Tl_{16}^{10-}]$ layer with a larger gap. The two frontier S bands around −5.4 eV that start around −6 eV, only ∼0.1 eV above the A bands, are essentially non-bonding or weakly antibonding, and their filling does not cause a substantial decrease in the network bonding. In fact, the evident requirement of tight packing of alkali-metal cations in the present structure together with closed shell bonding in Tl_{11}^{7-} afford an intermediate VEC of 56 and a $^2_\infty[Tl_{16}^{8-}]$ anion framework with an open band. Since either an exo-bond or a shared edge is generally considered to reduce the cluster charge by one

(31) Hoffmann, R. *J. Chem. Phys.* **1963**, *39*, 1397.
(32) Whangbo, M.-H.; Hoffmann, R.; Woodward, R. B. *Proc. R. Soc. London* **1979**, *A366*, 23.
(33) Pyykkö, P. *Chem. Rev.* **1988**, *88*, 563.
(34) Llusar, R.; Beltrán, A.; Andres, J.; Silvi, B.; Savin, A. *J. Phys. Chem.* **1995**, submitted.
(35) Blase, W.; Cordier, G.; Müller, V.; Häussermann, U.; Nesper, R.; Somer, M. *Z. Naturforsch.* **1993**, *48B*, 754.
(36) Hughbanks, T.; Hoffmann, R. *J. Am. Chem. Soc.* **1983**, *105*, 3528.

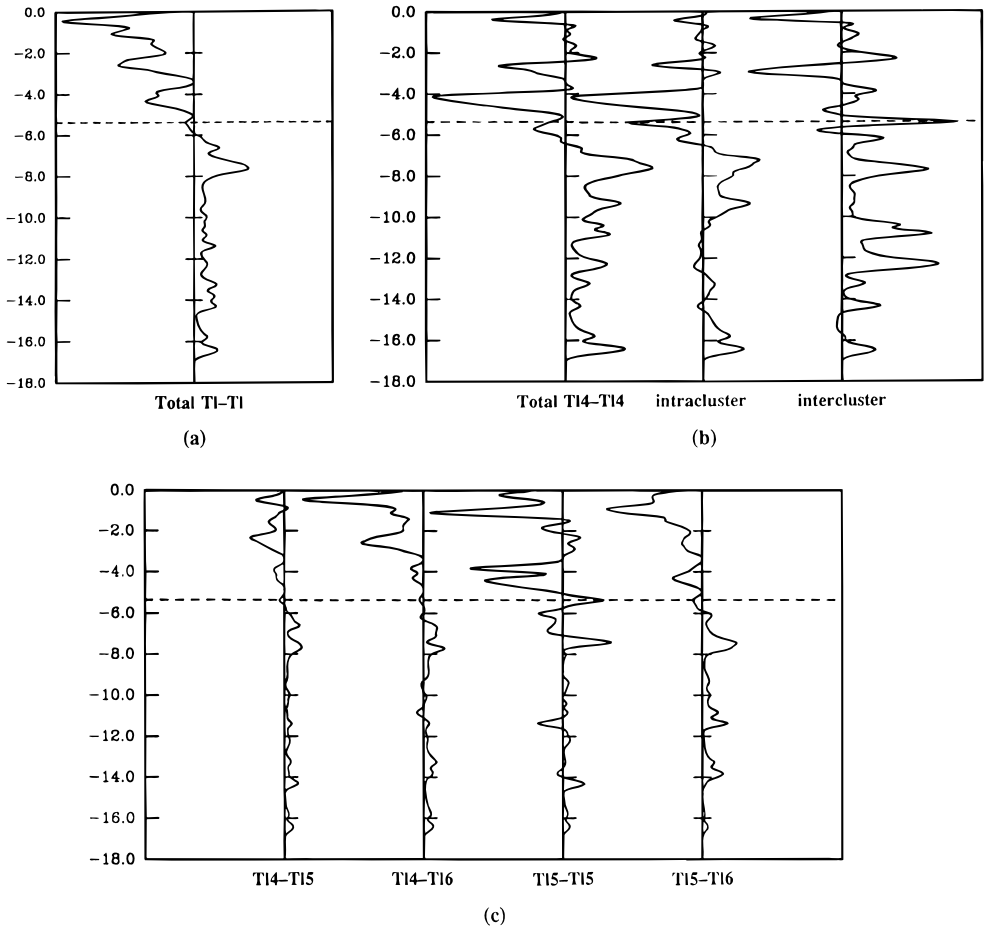

Figure 9. COOP curves evaluated for atom pairs in the condensed thallium layer in $Rb_{15}Tl_{27}$: (a) total Tl−Tl; (b) total Tl4−Tl4 and its decomposition into 3.319 Å intracluster and 3.073 Å intercluster components; (c) the rest of Tl−Tl bond types within the layer.[18]

Table 5. Dependence of the Fermi Energy and Overlap Populations upon Valence Electron Count for the Condensed Layer in $Rb_{15}Tl_{27}$

	valence electron count						
	53	54	55	56 (obsd)	57	58	59
E_F (eV)	−6.00	−5.95	−5.64	−5.37	−5.36	−5.00	−4.62
tot. Tl−Tl of the layer	0.219	0.220	0.219	0.217	0.216	0.215	0.210
tot. Tl4−Tl4	0.226	0.226	0.218	0.214	0.213	0.212	0.202
intracluster Tl4−Tl4	0.167	0.166	0.160	0.150	0.134	0.129	0.119
intercluster Tl4−Tl4	0.345	0.346	0.334	0.344	0.371	0.379	0.370
Tl4−Tl5	0.208	0.210	0.211	0.211	0.207	0.206	0.207
Tl4−Tl6	0.191	0.190	0.192	0.191	0.191	0.186	0.186
Tl5−Tl5	0.098	0.081	0.084	0.093	0.114	0.134	0.093
Tl5−Tl6	0.297	0.302	0.295	0.290	0.289	0.281	0.278

each,[37,38] addition of three exo-bonds and three shared edges to the Tl_{11}^{7-} skeleton should result in a Tl_{11}^{-} configuration. However, since each shared edge also results in the loss of one Tl and one 6p electron, three more electrons are required to stabilize the fragment, namely, $Tl_{11}^{-} - 3Tl + 3\,e^{-} = Tl_8^{4-}$, or Tl_{16}^{8-} per cell. The present structure again demonstrates how the cluster distortion, formation of exo bonds, and fusion of cluster units can be effective to reduce the cluster charge and hence produce a relatively stable phase.

The Fermi level at −5.37 eV for the observed VEC of 56 cuts through the two *S* bands (Figure 7). The higher lying is relatively flat and gives rise to the high DOS near E_F (Figure 8). The local DOS in Figure 8 also indicates that waist-capping Tl4 atoms have the largest overall contributions to the total DOS here while the shared Tl5 atoms order next and end-capping Tl6 atoms are the smallest, consistent with the condensation of the layer and the bonding discussed below. The observed Pauli-paramagnetic and metallic properties are in accord with the calculated band structure with partially filled bands and a nonzero DOS at the Fermi energy within the layer. Similar properties were also observed for A_8Tl_{11}, in which the electron from an extra cation is presumably delocalized over the double alkali-metal layers, as described by a $(A^+)_8Tl_{11}^{7-}e^-$ formulation.[16,29]

Since the waist Tl triangle undergoes significant contraction from the isolated to the condensed Tl_{11} unit and a new short intercluster Tl4−Tl4 connection is also established, the energy of the bands, especially those related to the waist Tl4 atoms, will change accordingly with respect to the isolated Tl_{11}^{7-} MO diagram. From the numerous well-dispersed bands shown in Figure 7, the strong intercluster (or intercell) interactions are obvious, as expected for an extended structure. (As a comparison, calculations performed on the full isolated K_8In_{11} structure gave very flat bands.[34,35]) The largest dispersion occurs in the *A* band (a″ symmetry at Γ) around −7 eV with a

(37) Teo, B. K.; Longoni, G.; Chung, F. R. K. *Inorg. Chem.* **1985**, *23*, 1257.
(38) Mingos, D. M. P. *Inorg. Chem.* **1985**, *24*, 114.

bandwidth of 0.68 eV. This band has significant p_z contributions from Tl4 atoms, all in-phase among themselves at the zone center Γ and also with other p_z orbitals in the neighboring Tl5 and Tl6 atoms. The next-most dispersed band is the *S* band (a′ symmetry at Γ) around −5.7 eV with a bandwidth of 0.47 eV, which has significant p_x and p_y contributions from Tl4 atoms and presents in-phase intercluster Tl4−Tl4 interactions but out-of-phase intracluster Tl4−Tl4 bonds, as illustrated through the variations of their corresponding overlap populations with different VECs (Table 5, Figure 9b). The very slight overlap between the energy of this band and next higher *S* band (around −5.3 eV, near E_F) is not only important in understanding properties of the phase but also critical for the condensation of the layer in terms of bonding. Significant net bonding for intercluster Tl4−Tl4 and shared Tl5−Tl5 are gained through both occupation of bonding states in the higher *S* band (near M) and reduction of antibonding effects in the lower *S* band near the K-point. Also interesting is the difference in the COOP curve of the intercluster Tl4−Tl4 bond from the others in the 6s-band region, Figure 9 (<−8.0 eV); the significant bonding amplitudes around −12 eV seem to insinuate that the 6s lone pair of the waist Tl atom, which is inert in the isolated Tl_{11}^{7-} unit, has been oxidized to form exo-bonds in the condensed layer. The overlap population for the shortest intercluster Tl4−Tl4 bond (3.07 Å) is the greatest among all bond types, a predictable result for extended Hückel calculations because the technique involves distance-sensitive overlap integrals. However, the significantly larger overlap population of this bond than others, together with the above bonding description, appears to establish its critical role in the layer condensation.

In order to explain the shift of the waist Tl4 atom from the center of the Tl5 rectangular face (Figure 1), band calculations were also carried out on a layer composed of hypothetical Tl_{11} (D_{3h}) fragments with all Tl4−Tl5 bond distances identical (3.255 Å). The overall band structure and bonding picture remain basically the same as those calculated for the observed geometry, as they should. The important thing about this calculation is that the equidistant (but symmetry inequivalent) Tl4−Tl5 bonds still classify into two types in terms of overlap populations. For the observed VEC = 56, the larger overlap population (0.231) corresponds to the shorter 3.216 Å bond in the real structure while the smaller (0.184) is for the longer 3.422 Å bond. This strongly suggests that the shift of Tl4 from the center of the Tl5 face pertains to better overall bonding (or orbital orientations) for the Tl4 atoms. Specifically, the displacement away from the interfragment Tl4−Tl4 bond is to avoid too short a distance (or too overly dominant a bond) and thus to assure appropriate bonding with other neighbors. The counteracting bonding character between intra- and intercluster Tl4−Tl4 bonds at E_F is probably also related to the distortion. Also noteworthy from calculations on both the hypothetical and observed geometries is that the overlap population for the relatively long Tl5−Tl6 bond is instead the next-largest, an indication of its importance in binding the layer together. In this sense, the observed $^2_\infty[Tl_{16}^{8-}]$ layer can be viewed composed of three sub-layers with critical Tl4−Tl4 bonding in the middle and Tl5−Tl6 on both sides.

Tuning of electron counts in the structure seems possible in terms of the band structure and overlap populations (Figures 7 and 9 and Table 5). Electron occupation around the Fermi energy affects mostly Tl4−Tl4 and Tl5−Tl5 bonding states while the rest are only slightly perturbed. This is related to the sharing or interconnection features of these atoms between the Tl_{11} units that are strongly associated with the condensation process. Up to two more electrons (VEC = 58, E_F = −5.0 eV) might be added to the aforementioned *S* band around −5.3 eV because, while this band remains basically nonbonding, the next *A* band above around −4.7 eV is strongly antibonding. The present layered framework might still remain favorable on such reduction because, despite the slight decrease of total Tl−Tl overlap population, the bonds mainly responsible for the condensation, intercluster Tl4−Tl4 and the shared Tl5−Tl5, are strengthened in terms of the increased overlap populations. The band structure also suggests that a tuned compound would be a semiconductor with an indirect band gap of ∼0.3 eV between the K and Γ points. However, this conclusion is probably not true because of the approximations inherent to the calculations. The alkali-metal valence electrons are unlikely to be completely localized on the thallium substructure, rather a minor participation of alkali-metal orbitals with filled thallium states may allow appreciable time-average electron delocalization and hence still yield a poor metallic behavior, as observed with most isolated cluster phases.[18,39] The most likely site for the electronic tuning is evidently Rb4, which *might* be replaced by a divalent (e.g., Ba^{2+}) or trivalent (e.g., La^{3+}) cation. The problem with such substitution is that these cations are probably too small to be bound effectively within the cavity. Doping the layer with Pb might be another choice. Instead of adding more electrons to the thallium substructure, electrons might be also taken away from it in terms of the optimum VEC of 54 via doping the layer with Cd or Hg. In any case, the tuned compound would be a Zintl phase after two electrons are either added to or subtracted from the layer because the band structure for either indicates a closed-shell bonding picture.[40] Further research is in progress.

Since the HOMO at −6.42 eV in the isolated Tl_{11}^{7-} cluster is quite low with respect to the an E_F of −5.37 eV for the condensed $^2_\infty[Tl_{16}^{8-}]$ anion layer, suitable coulombic energies of "solvation" must be necessary for both to have consistent Fermi energies. In fact, a band calculation including both condensed and isolated Tl_{11} components gave essentially the same bonding pictures for both portions and E_F = −5.72 eV at VEC = 96. The antibonding states of the isolated Tl_{11} cluster are not involved in the Fermi surface although the lowest bonds among these are very close to E_F. The possibility of electron transfer from the condensed layer to the isolated clusters is thus apparently excluded, consistent with bonding intuition. However, the Fermi energy calculated here is high because of, first, the neglect of alkali-metal cations and, second, the one-electron approximation of the extended Hückel theory. Electron correlations will lower the energy of all bands when the anion charge is reduced.[41] More sophisticated calculations would definitely help to better understand the packing and electronic balance in this structure, especially between the isolated and condensed Tl_{11} units.

Acknowledgment. We thank G. J. Miller, J. D. Martin, and L. M. Hoistad for discussions about the band calculations, and J. Ostenson for the measurements of magnetic susceptibility data.

Supporting Information Available: Tables of data collection and refinement details, positional and distance data for $Cs_{15}Tl_{27}$ and $Rb_{14}CsTl_{27}$, anisotropic displacement parameters for all three, and a drawing of the cation distributions about the isolated Tl_{11}^{7-} and condensed Tl_{11} units (5 pages). Ordering information is given on any current masthead page.

IC951086D

(39) Corbett, J. D. In *Chemistry, Structure and Bonding of Zintl Phases and Ions*; Kauzlarich, S., Ed.; VCH Publishers, to be published.
(40) Hughbanks, T. In *Inorganometallic Chemistry*; Fehlner, T., Ed.; Plenum Press: New York, 1992; p 291.
(41) Hoffmann, R. *Solids and Surfaces, A Chemist's View of Bonding in Extended Structures*; VCH Publishers, Inc.: New York, 1988; p 68.